Comprehensive Meteorological and Hydrological Drought Risks Under Changing Environment on the Wanquan River Basin, Southern China

Dan Li
Sun Yat-Sen University
Bingjun Liu (liubj@mail.sysu.edu.cn)
Sun Yat-Sen University https://orcid.org/0000-0002-9393-0674
Changqing Ye
Hainan University

Research Article

Keywords: Meteorological drought, Hydrological drought, Changing Environment, Wanquan River Basin

Posted Date: March 21st, 2022

DOI: https://doi.org/10.21203/rs.3.rs-1105479/v1

Abstract

Drought is one of the most frequent and devastating natural disasters. Based on future climate scenarios and land use/land cover (LULC) patterns, this study employed the copula framework to calculate the probabilities of meteorological drought risk based on downscaled data as well as hydrological drought risks based on SWAT model simulation data for the next 30 years (2021-2050) in the Wanquan River Basin (WRB), and meanwhile, the relationship between hydrological and meteorological droughts was revealed by correlation analysis and cross wavelet transform (XWT). The results are as follows: (1) In the next 30 years, the risk of intra-seasonal meteorological drought (short-term drought) in the WRB is high at a probability of 40%-70%, while the risk of inter-seasonal meteorological drought is relatively small at a probability of close to 30%; (2) Compared with meteorological drought, the risk of intra-seasonal hydrological drought is small, but the probability of inter-seasonal hydrological drought (medium or long term drought) is 30%-50%, and the risk of hydrological drought in the upstream is greater than that in the downstream; (3) The future meteorological and hydrological droughts in the WRB are significantly and positively correlated, and that hydrological drought lags behind meteorological drought.

1. Introduction

Drought is one of the recurring natural disasters with complex and multifaceted causes and can occur in any climate region (Chang et al., 2016; Mishra and Singh, 2010). Major drought events across the globe have been documented over the past decades, such as the 2000-2018 drought in the Southwest of North America, which was the second worst drought globally since the year 800 (Williams et al., 2020), and the 2002-2008 water depletion in northern India due to unsustainable extraction of groundwater for irrigation. Unlike other disasters, drought is a complex and integrated phenomenon that develops slowly and imperceptibly, so it is difficult to predict and track, and can negatively affect water resources, food, environment, as well as human and socioeconomic activities (Van Loon et al., 2016; Wu et al., 2021).

Generally, droughts are classified into meteorological drought, hydrological drought, agricultural drought and socioeconomic drought (Van Loon, 2013; Van Loon et al., 2016). Among them, meteorological and hydrological droughts are the main types of drought events, as agricultural droughts and socio-economic droughts are mainly caused by the persistence of meteorological and hydrological droughts. The root cause of meteorological drought is the shortage of precipitation. The current studies on meteorological drought is mainly focused on the monitoring, evaluation, quantification and risk of such drought, by developing new drought indices (e.g. based on copula, linear combination, principal component analysis, fuzzy set and entropy theory drought index) to capture drought events more accurately and evaluate drought risk more comprehensively (Chang et al., 2016; Huang et al., 2021; Rajsekhar et al., 2015; Sadegh et al., 2017; Zhang et al., 2019). What is more, meteorological drought risk assessment based on drought characteristics (drought duration, severity, and frequency), such as Gu et al. (2020) based on drought duration and severity to assess meteorological drought risk, and Xu et al. (2015) based on drought duration, drought severity, and affected areas to analyze drought frequency in Southwest China. When meteorological drought develops to a certain extent, the imbalance between surface water and groundwater reduces streamflow and thus induces hydrological drought, and meanwhile hydrological drought is also considered as a thorough drought (Wu et al., 2017). Hydrological drought is directly related to social water supply (Xu et al., 2019), so recent research on hydrological drought

concentrates on the construction of hydrological drought index, evolution, propagation and hydrological drought risk (Li et al., 2020; Wu et al., 2018a; Wu et al., 2019). The evolution of hydrological drought is more complicated under changing environments, and drought propagation is usually quantified by the response of hydrological drought to meteorological drought, extracting the propagation time from meteorological drought to hydrological drought to quantify the drought propagation process. However, drought propagation not only occurs among difference drought types, but also within the same drought type. For example, Zhang et al. (2016) used the change rate of water storage deficit to calculate the drought recovery. Parry et al. (2016a, b) proposed that hydrological drought propagation includes drought development and drought termination. And Wu et al. (2018) used mathematical expressions to quantify the internal propagation of hydrological drought for hydrological drought development and recovery process.

Meteorological drought develops faster and hydrological drought is the continuation and development of meteorological drought, caused by the persistence of meteorological drought, with these two type of droughts reflecting different stages of drought development (Wu et al., 2017). Combining meteorological drought and hydrological drought can provide a thorough understanding of drought characteristics. In addition, the quantification of droughts is a prerequisite for analyzing drought risk. There is a close relationship between meteorological and hydrological droughts (Wu et al., 2018b; Wu et al., 2017), and it is believed that the former is the main factor behind the latter. The propagation threshold (PT) from meteorological to hydrological drought is an essential feature of drought propagation, and is of paramount importance for drought mitigation and prevention (Lorenzo-Lacruz et al., 2013; Wu et al., 2021). Three methods are adopted to characterize PT from meteorological to hydrological drought, i.e. run theory, correlation analysis, and non-linear response method (Wu et al., 2021). As a common method to obtain drought thresholds, correlation analysis establishes correlations between hydrological drought indices at a certain timescale and meteorological drought indices at different timescales by Spearman's and Pearson's correlation coefficients (Wu et al., 2017; Xu et al., 2019). Additionally, it determines the PT from hydrological to meteorological drought by using the highest correlation coefficients. A more comprehensive analysis of the relationship between hydrological and meteorological drought can advance the understanding of causes of drought and is of great significance for early warning of hydrological drought (Huang et al., 2017; Wang et al., 2020; Xu et al., 2019) .

As the third largest river in Hainan Province, the Wanquan River plays an important part in the development of Hainan Province. The basin has a high forest cover with abundant tropical forest resources, rubber plantations, pulp forests and tropical cash crops such as areca nut. However, the uneven intra-annual distribution of precipitation within the river basin and frequent droughts have caused tremendous losses to tropical cash crops. Therefore, the objective of this study is to probe into the evolution of meteorological drought and hydrological drought in the WRB under future climate change and land use change, and to reveal the correlation of meteorological and hydrological drought.

2. Study Area And Data Sources

2.1. Study area

The WRB is located in the east-central part of Hainan Island, China (109°37'-110°38'E, 18°46'-19°31'N) (shown in Figure 1). The natural resources and geographical location of WRB are the most important ecological

shelters in Hainan Province, and the ecological environment of the basin plays a pivotal role in the national economy, social development and building of free trade port in Hainan Province. The WRB hosts 5 major cities with a total population of 1.78 million and a GDP of US$8.371 billion across such cities as Qiongzhong, Dingan, Tunchang, Qionghai and Wanning. Wanquan River originates from Fengmenling in Wuzhishan and flows eastward into the South China Sea, with a total length of 163 km, a basin area of 3,693 km^2, and an annual river runoff of 5.83 billion m^3 (Zhao et al., 2019). Situated in a tropical monsoon climate zone, Wanquan River has an average annual temperature of 24°C and a multi-year average precipitation of 2,300 mm. The precipitation is unevenly distributed in a unimodal curve within the year. For example, 87% of precipitation occurs in the rainy season (May-November), whereas only 13% in the dry season (December-April). The extremely uneven distribution of precipitation contributes to frequent drought events in the WRB. The main types of drought in the basin were winter-spring drought, a historically rare drought that occurred in 1976-1977, which is the longest and severest abnormal drought in history, 80% of the rivers in the basin had been cut off. The Wanquan River had the lowest water level and lowest flow in history, and more than 80% of the reservoirs dried up. As a result, agriculture faced great difficulties. Specifically, 43% of the crops were drought-stricken and more than 50% of the planted area was lost. In 1994-1995, a winter-spring drought hit Ding'an, Qiongzhong and Wanning, lasting for 100-164 days and affecting large areas. This was particularly worse in April-May, with continuous high temperatures, high evaporation, rapid decline of water levels in rivers and reservoirs, and rapid development of the drought. Hainan Province suffered "the hottest year in history ", with high temperature and less rain in the spring and summer seasons of 2015, and the basin suffered a severe drought hazard. Severe drought events have occurred in the WRB, but still no effective early warning was in place. Additionally, socio-economic development renders urbanization inevitable, and the transformation of the underlying surface by human activities, which in turn affects the hydrological processes, should not be underestimated. Owing to specific climatic conditions, as well as the dynamics of LULC of the region, the mechanisms of drought events therein may well have been influenced. As a result, the WRB was selected as the study basin to explore the impacts of climate change and LULC on drought events.

Figure 1 is here

2.2. Data sources

2.2.1. NASA Earth Exchange Global Daily Downscaled Projections (NEX-GDDP)

To obtain future global climate model (GCM) data at the basin scale, downscaled data from BCC-CSM1-1 within the CMIP5 dataset were selected, which has a spatial resolution of 0.25°x 0.25° and contains daily precipitation, maximum and minimum temperatures for two emission scenarios, RCP4.5 and RCP8.4, these data were obtained from NEX-GDDP (https://cds.nccs.nasa.gov/nex-gddp/). These two emission scenarios serve as the core datasets of the CMIP5 model and can be employed as the primary assessment study (Sun et al., 2019; Taylor et al., 2012). This downscaled data can more accurately characterize the future climate for a smaller area, so the meteorological data from this dataset for 2021-2050 were selected to drive the calibrated SWAT model to simulate future streamflow processes, and the streamflow data obtained were used to predict the probability of future hydrological drought risk.

2.2.2. Observed data

To construct the SWAT model for the WRB, spatial data and hydrometeorological data are required, and the details and sources of the data are as follows. The hydrometeorological data include daily precipitation data from 22 precipitation stations (blue circles in Figure 1) from 1967-2014 from the Water Department of Hainan Province. The data about two meteorological stations, including maximum and minimum temperature, wind speed, relative humidity and solar radiation, were obtained from the China Meteorological Data Service Centre (http://www.nmic.gov.cn). These meteorological data were used to create the meteorological database for the SWAT model. Daily streamflow data from 1967-2014 for two hydrological stations in the basin (red triangles in Figure 1) were acquired from the hydrological yearbooks compiled by the Hydrology Bureau of Hainan Province and used to calibrate and validate the SWAT model. The multi-year average precipitation in the basin was calculated by a simple arithmetic mean method.

The spatial data include digital elevation model (DEM) data obtained from the geospatial data cloud at 30m resolution (shown in Figure 1). The five sets of data on LULC at 30m resolution for 1980, 1990, 2000, 2010 and 2015 were obtained from TM remote sensing data after geometric correction and radiometric correction, through supervised classification and manual interpretation. They were provided by the Institute of Geographic Sciences and Natural Resources Research, Chinese Academy of Sciences (IGSNRR) (http://www.resdc.cn). The DEM map and land use map were kept at the same resolution to better describe the conditions of the underlying surface, which can simulate the streamflow process more accurately. The soil data of the study area were provided by the 1:1 million soil dataset from Nanjing Institute of Soil Research, Chinese Academy of Sciences. All spatial data were converted to the same geographic and projected coordinates and employed to construct the SWAT model.

3. Methodology

The aim of this research is to study the meteorological drought risk and hydrological drought risk and their relationship under future climate and land use scenarios. For the meteorological drought risk, which involves calculating standardized precipitation index (SPI) based on GCM downscaled meteorological data, extracting drought characteristics by run theory, and constructing a regional meteorological drought risk model using copula function. For hydrological drought risk, which involves the use of future meteorological data and CA-Markov models to predict future land use scenarios to construct a regional future SWAT model for predicting future hydrological drought. Similarly, hydrological drought characteristics extracted using run theory, then the copula function is used to construct a regional hydrological drought risk model. Finally, XWT is used to explore the link between meteorological drought and hydrological drought, and Pearson correlation coefficient (PCC) is used to identify PT from meteorological drought to hydrological drought. The flow chart of this study is shown in Figure 2.

Figure 2 is here

3.1. Model for predicting future LULC

(1) CA-Markov model

CA-Markov models can be used to model temporal and spatial patterns of land use prediction. For starters, based on the current status of an event, the Markov model calculates the transition matrix between different

states with Markov chains, aiming to predict the status of a future period. Afterwards, the CA model is characterized as a model for network dynamics with discrete time, space and state, centering on the interactions of cells for different spatio-temporal features, with powerful spatial computational simulation capability, particularly suitable for dynamic simulation and spatial presentation of self-organizing functional systems. Regarding the prediction of land use, the Markov model gives priority to the prediction of the amount of land use change, but neither can it be spatially expressed nor can it present the spatial distribution of each type of land change. In contrast, the CA model is able to express the spatio-temporal dynamic evolutionary process of complex spatial systems and can overcome the deficiencies in the Markov model (Wickramasuriya et al., 2009). Therefore, the CA-Markov model integrates the advantages of Markov chains for long-term prediction of time and the ability of the CA model to simulate complex changes in space, and applies the quantitative land use transition matrix derived from the Markov model to the CA model. In this way, the central cell can determine whether to convert more reasonably on the basis of transition probability, with high prediction accuracy, which is extensively used by domestic and foreign scholars to predict land use change (Halmy et al., 2015; Zhang et al., 2020). Based on the advantages mentioned above, this paper applied the CA-Markov model to predict the future LULC.

(2) Accuracy assessment

Kappa coefficient can effectively assess the spatial consistency of the CA-Markov model simulation results with observed data from an overall perspective, and are widely applied in studies such as accuracy check of land use change simulation as well as interpretation and evaluation of remote sensing image (Ghosh et al., 2017). The Kappa coefficient is calculated as follows:

$$\text{Kappa} = \frac{p_o - p_c}{1 - p_c} \qquad (1)$$

p_o is the proportion of correctly simulated raster cells, and p_c is the proportion of correctly simulated cells at random. The range of Kappa coefficient draws from the literature, and it is generally believed that Kappa > 0.6 has a greater consistency, while Kappa > 0.8 has a significant simulation effect.

3.2. SWAT hydrological model

The SWAT model is a semi-distributed hydrological model developed by the United States Department of Agricultural Research Service (USDA-ARS), based on the principles of hydrological cycle and water balance for the simulation of streamflow generation and confluence processes in river basins. The SWAT model has the following characteristics: (1) It has a strong physical mechanism and its parameters are spatially distributed; (2) It can evaluate and predict the impact of land use changes on streamflow; (3) It can predict streamflow in areas with little or no measured hydrological and meteorological data; (4) It is a collection of numerous equations and intermediate variables, covering all aspects of precipitation, evaporation, infiltration, and streamflow formation, such as SCS curves and the Muskingum algorithm (Sun et al., 2019; Zhang et al., 2015). Based on these advantages, this paper adopted the SWAT model to simulate future streamflow and used the simulated streamflow to calculate future hydrological drought risk.

The SWAT model divides the WRB into 48 sub-watershed by loading DEM maps, land use maps, soil maps (Figure 3). Owing to the large number of parameters involved in the SWAT model, seven sensitive parameters

were selected based on the SWAT-CUP sensitivity analysis and employed to calibrate and validate the monthly streamflow from two hydrological stations, Jibao and Jiaji. SWAT-CUP automatically calibrates the selected parameters through 2,000 simulations, and decides whether to adjust the parameters to continue the simulation according to whether the criteria are met, and after the criteria are satisfied, the optimal parameter values are determined.

3.3. Standardized precipitation/streamflow drought index

In order to predict meteorological and hydrological drought, the selection of suitable meteorological and hydrological drought indices is of vital importance for the study results. Precipitation and streamflow are commonly used to characterize meteorological and hydrological droughts. The calculation steps are detailed as follows. The cumulative precipitation is calculated based on monthly precipitation data, and the precipitation is described by a specific cumulative probability density function over time, which is then converted into a standard normal distribution of actual SPI values using equal probability transformations. One of the merits of SPI is its ability to monitor and track meteorological droughts at different timescales. For instance, the 1-month and 3-month SPI indices are more sensitive to short-term droughts, while the 12-month and 24-month SPI indices can better capture the characteristics of long-term droughts (Wu et al., 2018b). In this study, standardized streamflow index (SSI) was employed to characterize hydrological drought, because the principles and advantages of SSI and SPI are similar, so we will not go into too much detail.

3.4. Identification of drought events

Run theory is a method used to extract drought characteristics, including drought onset, duration, severity, and termination. Among them, drought duration and severity are the major characteristics of drought duration (Chang et al., 2016). In light of the run theory, drought duration represents the period of time during which the drought index remains below the truncation level, and drought severity is defined by the cumulative drought indices throughout the drought duration. The SPI and SSI time series are standardized rather than direct measurements of precipitation and streamflow, and in this study, a threshold of -0.5 was selected to obtain sufficient drought events in order to reduce the uncertainty of sample size in the frequency analysis. Two truncation levels (-0.5, 0) were employed to extract drought duration and severity based on the SPI (SSI) drought classification (Wu et al., 2017). For a drought process with a drought duration equal to 1, if the 1-month drought index is less than -0.5, the corresponding month is considered drought; for two drought processes, if the interval is equal to 1 and this index is less than 0, they are combined into one drought process. Drought duration is the sum of the months where drought events occur, and drought severity is the sum of drought indices during droughts. In this paper, run theory and truncation level were employed to extract two indices of drought duration and severity to describe drought events.

3.5. Copula-based model for drought risk prediction

Conventional methods based on univariate time series are too subjective in conducting drought frequency study on drought risk. With the introduction of copula function to hydrology, the multivariate frequency analysis on drought characteristics has been developed more rapidly. The drought duration and severity extracted from the run theory are the primary characteristics of drought events, so this study effectively avoided these deficiencies by combining marginal distribution and the maximum probability of joint distribution function. 6 marginal distribution function were selected to determine the most appropriate one, and the summary

mathematical description of the marginal distribution functions is given in Table 1. In this paper, copula drought risk model was adopted to study the combined scenarios of drought duration and severity under the bivariate return periods of intra-seasonal scale and inter-seasonal scale. Additionally, 5 copula families were employed to determine the appropriate one, and details can be seen in Table 2. The steps are as follows. First, the marginal distribution functions of drought duration and severity were calculated separately. Second, the parameters of the marginal distribution functions were assessed using the maximum likelihood estimation, and the univariate distributions were fitted respectively. Finally, the joint distribution functions were tested using the root mean square error (RMSE), the Akaike information criterion (AIC) and the Bayesian Information Criterion (BIC). The smaller the RMSE, AIC and BIC values, the better the function fit.

Table 1

Summary mathematical description of the probability distribution functions

Name	Mathematical description of PDF	parameter
Birnbam saunders	$\frac{1}{\sqrt{2\pi}}\exp\left\{-\frac{\left(\sqrt{x/\beta}-\sqrt{\beta/x}\right)^2}{2\alpha^2}\right\}\left\{\frac{\left(\sqrt{x/\beta}+\sqrt{\beta/x}\right)}{2\alpha x}\right\}$	$for\ x>0,$ $\beta>0,\ \alpha>0$
Exponential	$y=\frac{1}{\mu}e^{\frac{-x}{\mu}}$	$\mu>0$
Generalized extreme value	$y=(\frac{1}{\sigma})exp\left[-\left(1+\kappa\frac{x-\mu}{\sigma}\right)^{\frac{-1}{\kappa}}\right]\left(1+\kappa\frac{(x-\mu)}{\sigma}\right)^{-1-\frac{1}{\kappa}}$ $for\ 1+\kappa\frac{(x-\mu)}{\sigma}>0$	$\kappa\neq0$
Generalized pareto	$y=(\frac{1}{\sigma})\left(1+\kappa\frac{x-\theta}{\sigma}\right)^{-1-\frac{1}{\kappa}}$	$\kappa>0,\ \theta<0;\ \kappa<0,$ $\theta<x<\theta-\sigma/k$
Inverse gaussian	$\sqrt{\frac{\lambda}{2\pi x^3}}\exp\left[-\frac{\lambda}{2\mu^2 x}(x-\mu)^2\right]$	$\mu>0,\ \lambda>0$
Lognormal	$y=\frac{1}{x\sigma\sqrt{2\pi}}\exp\left[-\frac{(logt-\mu)^2}{2\sigma^2}\right]$	$-\infty<\mu<\infty,\ \sigma\geqslant0$

4. Results

4.1. Prediction of meteorological drought risk

(1) Selection of the optimal marginal distribution

Drought duration and severity are the main features characterizing drought events, and they are extracted form SPI based on the run theory. To obtain the suitable marginal distribution function for drought, distribution

functions, such as exponential distribution, lognormal distribution and gamma distribution, were employed to fit drought duration and severity in both RCP4.5 and RCP8.5 scenarios. Finally, the marginal distributions with the goodness of fit (GOF) were selected based on the minimum AIC and BIC, and the results are shown in Table 3. The four fitting functions for the duration of meteorological drought under PJB4.5, PJB4.5, PJB8.5 and PJJ8.5 scenarios were generalized extreme value, inverse gaussian, inverse gaussian, and generalized pareto, respectively, while the fitting functions for drought severity were all exponential, and the parameters of each distribution function can be observed in Table 3. Besides, the Kendall's rank correlation coefficient and Spearman's rank correlation coefficient were also adopted to test the correlation between drought duration and severity before establishing the joint distribution function. As shown in Table 3, the Kendall's rank correlation coefficients were all above 0.68, while the Spearman's rank correlation coefficients were all greater than 0.8. The correlation coefficients all passed the significance test of $\alpha = 0.05$, suggesting that drought duration and severity were highly correlated. Consequently, the copula function can be employed to determine the joint distribution function of drought duration and severity in the WRB.

Table 2

Summary of selected copula families and their mathematical description

Name	Mathematical description	Parameter range
Normal-copula	\int_{{ - \infty }}^{{{\emptyset ^{ - 1}}(\mu)}} {\int_{{ - \infty }}^{{{\emptyset ^{ - 1}}(\nu)}} {\frac{1}{{2\pi \sqrt {1 - {\theta ^2}} }}} } \exp \left({\frac{{2\theta xy - {x^2} - {y^2}}}{{2(1 - {\theta ^2})}}} \right)dxd{y^b}	\theta \in [- 1,1]
t-copula	\int_{{ - \infty }}^{{{\text{t}}_{{{\theta _2}}}^{{ - 1}}(\mu)}} {\int_{{ - \infty }}^{{{\text{t}}_{{{\theta _2}}}^{{ - 1}}(\nu)}} {\frac{{\Gamma ((\theta +2)/2)}}{{\Gamma ({\theta _2}/2)\pi {\theta _2}\sqrt {1 - {\theta _1}^{2}} }}{{(1+\frac{{{x^2} - 2{\theta _1}xy+{y^2}}}{{{\theta _2}}})}^{({{\theta _2}+2)/2}}} } dxd{y^c}	{\theta _1} \in [- 1,1],{\theta _2} \in (0,\infty)
Clayton-copula	\hbox{max} {({\mu ^{ - \theta }}+{\nu ^{ - \theta }} - 1,0)^{ - 1/\theta }}	\theta \in ({\text{-1}},0) \cup (0,\infty)
Frank-copula	- \frac{1}{\theta }\ln \left[{1+\frac{{(exp(- \theta \mu) - 1)(exp(- \theta \nu) - 1)}}{{\exp (- \theta) - 1}}} \right]	\theta \in ({\text{-}}\infty ,0) \cup (0,\infty)
Gumbel-copula	\exp \left\{ { - {{\left[{{{\left({ - \ln (\mu)} \right)}^\theta }+{{(- ln(\nu))}^\theta }} \right]}^{1/\theta }}} \right\}	\theta \in [1,\infty]

(2) Selection of the optimal copula functions

Through the analysis of marginal distribution functions, the copula functions could be used to determine the joint distribution of meteorological drought duration and severity in the basin. Therefore, five copula functions were selected to determine the joint distribution functions of meteorological drought duration and severity. The results are presented in Table 4. Although all copula functions showed good agreement in the formulation of the joint distribution, the optimal copula functions for meteorological drought duration and drought severity were selected based on the GOF, and the optimal copula for each scenario using bolded font. For the drought duration and severity in the WRB, Gumbel-copula dominated in the selected optimal joint combinations, among

which, the optimal joint distribution functions of PJB4.5, PJB8.5, and PJJ8.5 scenarios are all Gumbel-copula, and the PJJ4.5 scenario is t-copula. The parameter estimates of the copula function are shown in Table 4.

Based on the copula selected from the GOF, the probabilities calculated based on the fitted distribution function were used to plot the scatter plots of drought duration and drought severity in Figure 4. It can be seen from the figure that the high probability part of drought duration and drought severity is well fitted, and the joint probability distribution values of the two go up with increasing drought duration and drought severity. This also confirms that the high probability of drought duration and that of drought severity move in the same direction, while the low probability part is poorly fitted. There are two reasons behind this conclusion: 1) Limited time series and insufficient drought events; 2) The SPI index is calculated for monthly precipitation data and the calculated drought durations are discrete in nature. Therefore, based on the above description, the best copula function based on each scenario is used for meteorological drought risk probability prediction.

Table 3

Fit error of marginal distribution of meteorological drought duration and severity.

Scenario	drought	Optimal distribution	Parameter	AIC	BIC	Kendall rank	Spearman rank
PJB4.5	duration	generalized extreme value	κ=4.46, σ=0.16,μ=1.04	46.79	52.07	0.68**	0.81**
	severity	exponential	μ=1.66	131.41	133.17		
PJJ4.5	duration	inverse gaussian	μ=2.67, λ=4.38	154.91	158.43	0.75**	0.88**
	severity	exponential	μ=1.66	131.62	133.38		
PJB8.5	duration	inverse gaussian	μ=2.21, λ=4.72	148.53	152.27	0.7**	0.82**
	severity	exponential	μ=1.48	135.55	137.43		
PJJ8.5	duration	generalized pareto	κ=22.17, σ=0.001,θ=1.00	103.51	107.71	0.68**	0.8**
	severity	exponential	μ= 1.49	108.01	110.81		

Note: Regarding the meaning of letters in PJB4.5 and SJJ8.5, P and S stand for precipitation and streamflow, respectively; JJ and JB stand for Jiaji Station and Jiabao Station, respectively; 4.5 and 8.5 stand for RCP4.5 and RCP8.5 scenarios, respectively. "**" indicates that the correlation coefficient passed the test of α=0.05.

Table 4

Fit errors of copula functions for meteorological drought duration and severity

Scenario	Copula	RMSE	AIC	BIC	θ
PJB4.5	Clayton-copula	0.19	-304.17	-302.4	
	Frank-copula	0.15	-322.4	-320.63	
	Gumbel-copula	**0.12**	**-341.49**	**-339.73**	2.73
	Normal-copula	0.12	-339.54	-337.78	
	t-copula	0.12	-340.57	-337.05	
PJJ4.5	Clayton-copula	0.13	-336.43	-334.67	
	Frank-copula	0.11	-347.43	-345.67	
	Gumbel-copula	0.1	-359.75	-357.98	
	Normal-copula	0.09	-363.5	-361.74	
	t-copula	**0.09**	**-365.42**	**-361.9**	θ1=0.90, θ2=9.98
PJB8.5	Clayton-copula	0.13	-380.8	-378.93	
	Frank-copula	0.1	-403.05	-401.18	
	Gumbel-copula	**0.09**	-414.27	**-412.39**	2.21
	Normal-copula	0.09	-411.51	-409.64	
	t-copula	0.09	-414.6	-410.85	
PJJ8.5	Clayton-copula	0.2	-337.02	-335.15	
	Frank-copula	0.15	-367.76	-365.89	
	Gumbel-copula	**0.09**	**-418.47**	**-416.6**	2.38
	Normal-copula	0.12	-387.57	-385.7	
	t-copula	0.11	-395.06	-391.32	

Figure 4 is here

(3) Prediction of meteorological drought risk probability

After the marginal distribution function and the copula function were determined, the drought risk assessment model was used to predict the intra- and inter-seasonal meteorological drought risk probabilities for the next 30 years (2021-2050). The drought risk probabilities for the two greenhouse gas (GHG) emission models can be seen in Table 5. For meteorological drought risk, the probability of intra-seasonal drought occurrence under the three scenarios of PJB4.5, PJJ4.5 and PJB8.5 was 60%-70%, which indicates that intra-seasonal meteorological droughts are prone to occur in the WRB in the next 30 years. However, the risk of intra-seasonal drought for the PJJ8.5 scenario is relatively small at 42.6%. By contrast, the risk of inter-seasonal droughts under the four scenarios is relatively low, with a probability is about 30%, the PJB8.5 scenario with even small probability risk of 16.76%. Therefore, the probability of intra-seasonal droughts in the WRB in the next 30 years is high,

indicating that meteorological droughts are mostly short-term droughts. This is mainly determined by the climate of the basin, which is in a tropical monsoon climate with uneven distribution of precipitation within the year, with the rainy season (May-November) accounting for approximately 80% of the annual precipitation, so the main types of drought in the WRB were short-term droughts such as winter droughts and winter-spring droughts (Zhao et al., 2019). To better understand why short-term droughts are prone to occur in the WRB, six statistical coefficients were used for analysis herein, including nonuniformity coefficient (Cn), complete accommodation coefficient (Cc), concentration degree (Cd), concentration period (Cp), relative variation range (Cr), and absolute variation range (Ca). Please refer to (Lin et al., 2017) for detailed calculation steps about six statistical coefficients,. As shown in Table 6, the results of the uneven intra-annual distribution of precipitation are consistent with the risk of intra-seasonal meteorological drought, demonstrating that short-term droughts tend to hit the WRB.

Table 5

Probabilistic prediction of intra-seasonal and inter-seasonal meteorological drought risk

Scenario	PJB4.5	PJJ4.5	PJB8.5	PJJ8.5
Intra-seasonal	62.85	65.54	66.78	42.62
Inter-seasonal	27.25	27.56	16.76	32.78

Table 6

Intra-annual variation of precipitation in WRB

Scenario	Cn	Cc	Cp	Cd	Cr	Ca
PJB45	0.72	0.32	0.37	0.49	15.06	359.72
PJJ45	0.70	0.31	0.30	0.48	14.71	345.04
PJB85	0.66	0.30	0.41	0.46	13.83	316.22
PJJ85	0.65	0.29	0.33	0.45	13.11	289.87

4.2. Hydrological drought risk prediction

4.2.1. Prediction of LULC in the WRB

In this paper, we used the CA-Markov module in IDRISI software to simulate and predict the LULC following the principle of equal time interval, and simulated the LULC maps of 2000 to simulate those 1980 and 1990 to simulate. By taking 1990 as the base year and according to the land use transition matrix and land use suitability maps of 1980-1990 (similar to the land use over the past decade), we used the CA-Markov module to simulate the LULC maps of 2000, and compared and analyzed the similarity between the measured and simulated land use maps of the WRB in 2000 with the Crosstab module in IDRISI. The Kappa coefficient was 0.9. Similarly, the LULC maps of 1990 and 2000 were used to predict those of 2010 whose validated Kappa coefficient was 0.91. The results demonstrate that the Kappa coefficients of the predicted and measured maps for both periods are greater than 0.8. Additionally, the simulation results are presented in Figure 5, suggesting

that the simulation results are highly reliable, so the CA- Markov model can be adopted for prediction and simulation of land use in the WRB.

Therefore, by using the above validated CA-Markov prediction and simulation program and regarding 2015 as the start year, the land use transition matrix and suitability map was calculated in light of the historical land use maps of 1980, 1990 and 2000, respectively. Meanwhile, 15, 25 and 35 CA iterations were selected accordingly to predict the projected land use maps for 2030, 2040 and 2050 (shown in Figure 6). The overall spatial distribution of land use in 2030, 2040 and 2050 is basically the same as that in 2015, but there are clear changes in each land use type within them.

Figure 5 is here

Figure 6 is here

4.2.2. Calibration and validation of the SWAT model

In order to improve the accuracy of the model simulation for better understanding of the hydrological processes in the WRB, two major hydrological stations were selected for calibration and validation. The monthly streamflow of the basin from 2000 to 2010 were simulated with monthly scale as the time step, and the year 2000 was regarded as the model warm-up period to minimize experimental errors. Beyond that, to create initial conditions for model simulation, the years 2001-2005 were regarded as the model calibration period and 2006-2010 as the model validation period. The sensitivity analysis of the SWAT model parameters is presented in Table 7. The simulation and observation results of the SWAT model are shown in Figure 7. The measured streamflow, simulated streamflow and precipitation process of each month in the calibration and validation periods are relatively consistent, and the simulation results of the two hydrological stations have achieved satisfactory results. The R^2 values of Jiabao Station were 0.79 and 0.94 for the calibration and validation periods, respectively (Table 8), and the Ens coefficients were 0.67 and 0.81, respectively. Regarding Jiaji Station, the R^2 values and Ens coefficients were 0.83 and 0.60 for the calibration period, and 0.93 and 0.86 for the validation period, respectively. In general, the streamflow from the two hydrological stations met the requirements during the calibration and validation periods. In addition, the SWAT model can better simulate the hydrological processes affected by climate and land use changes in the WRB, and can be used to simulate and analyze the hydrological drought conditions in the WRB.

Table 7

Sensitivity parameters of the SWAT model

Parameter Name	Parameter definition	Calibrate method	Calibrate value	Order
CN2	The SCS curve number	R	-0.4817	1
ALPHA_BF	Base flow alpha factor (days)	V	1.4089	2
ESCO	Soil evaporation compensation factor	V	11.7706	3
GW_DELAY	Groundwater delay (days)	V	0.1927	4
GWQMN	Threshold depth of water in shallow aquifer required for return flow to occur (mm)	V	0.1276	5
SOL_AWC	Available water capacity of the soil	V	0.8681	6
GW_REVAP	Groundwater re-evaporation coefficient	R	-0.0527	7

Table 8

Calibration and validation results of streamflow simulation using the SWAT model

Station	Calibration		Validation	
	R^2	Ens	R^2	Ens
Jiabao station	0.79	0.67	0.94	0.81
Jiaji station	0.83	0.60	0.93	0.86

Figure 7 is here

4.2.3. Prediction of hydrological drought risk

(1) Selection of marginal distribution function

To obtain suitable marginal distribution of hydrological droughts characteristics, the SWAT model parameters obtained from the calibration and validation periods were used to predict future streamflow under RCP4.5 and RCP8.5 scenarios. In the next step, the hydrological drought index was calculated; the hydrological drought duration and drought severity were extracted by the run theory; and distribution functions (eg. exponential, lognormal, and gamma distributions) were used to fit the hydrological drought duration and drought severity. Marginal distribution with GOF was selected based on the minimum AIC and BIC, and the results are shown in Table 9. The fitting functions of hydrological drought duration and drought severity distribution under RCP4.5 and RCP8.5 scenarios are also presented in Table 9.

Table 9

Fit error of marginal distribution of hydrological drought duration and severity.

Scenario	drought	Optimal distribution	Parameter	AIC	BIC	Kendall rank	Spearman rank
SJB45	duration	generalized extreme value	κ=-0.22, σ=3.36, θ=1.00	137.51	142	0.78**	0.92**
	severity	lognormal	μ=-0.01, σ=1.34	115.19	118.18		
SJJ45	duration	generalized extreme value	κ=5.23, σ=2.25, μ=1.43	103.51	107.71	0.8**	0.92**
	severity	birnbaum saunders	β=1.00, α=1.64	108.01	110.81		
SJB85	duration	generalized pareto	κ=0.11, σ=3.24, θ=1.00	115.67	119.2	0.82**	0.93**
	severity	exponential	μ=2.88	100.73	101.9		
SJJ85	duration	generalized pareto	κ=24.23, σ=0.001, θ=1.00	36.2	40.08	0.82**	0.95**
	severity	generalized pareto	κ=1.96, σ=0.27,θ=0.001	95.61	99.5		

Note: "**" indicates that the correlation coefficient passed the test of α=0.05

(2) Selection of the optimal copula functions

The analysis of marginal distribution functions demonstrated that the copula functions could be used to determine the joint distribution of hydrological drought duration and severity in the basin, and the results are presented in Table 10. The optimal copula functions selected by GOF of each scenario were used to predict the probability of drought risk, and the probability distribution between hydrological drought duration and drought severity in WRB was plotted in Figure 8. It can be observed from the figure that the high probability part of hydrological drought duration and drought severity is well fitted, and the joint probability distribution values also show an increasing trend as drought duration and drought severity increase. By contrast, the low probability part is poorly fitted, resulting from the limited time series and the discrete durations of drought. A number of studies have also stressed the importance of joint probability, because joint probability is an important guide for the assessment of water resources systems and offers great values for drought risk assessment (Ayantobo et al., 2021; Shiau, 2006).

Table 10

Fit errors of copula functions for drought duration and severity

Scenario	Copula	RMSE	AIC	BIC	θ
SJB45	Clayton-copula	0.09	-273.97	-272.47	
	Frank-copula	**0.06**	**-303.19**	**-301.69**	12.83
	Gumbel-copula	0.06	-297.97	-296.48	
	Normal-copula	0.06	-296.74	-295.24	
	t-copula	0.06	-294.66	-291.67	
SJJ45	Clayton-copula	0.19	-304.17	-302.4	
	Frank-copula	0.15	-322.4	-320.63	
	Gumbel-copula	**0.12**	**-341.49**	**-339.73**	3.36
	Normal-copula	0.12	-339.54	-337.78	
	t-copula	0.12	-340.57	-337.05	
SJB85	Clayton-copula	0.09	-191.74	-190.56	
	Frank-copula	0.07	-199.45	-198.27	
	Gumbel-copula	0.06	-205.56	-204.38	
	Normal-copula	**0.06**	**-205.66**	**-204.48**	0.92
	t-copula	0.06	-203.6	-201.24	
SJJ85	Clayton-copula	0.06	-242.75	-241.45	
	Frank-copula	0.06	-243.31	-242.01	
	Gumbel-copula	0.06	-238.51	-237.21	
	Normal-copula	**0.06**	**-243.39**	**-242.09**	0.9
	t-copula	0.06	-241.35	-238.76	

Figure 8 is here

(3) Prediction of hydrological drought risk probability

After the marginal distribution function and copula function were determined, the drought risk assessment model was employed to project the probabilities of intra-seasonal and inter-seasonal drought risk for the next 30 years (2021-2050). Table 11 demonstrates the probabilities of drought risk for the two GHG emission models. For hydrological drought, the probability of intra-seasonal hydrological drought risk is 35%-60%, and that of inter-seasonal hydrological drought risk is 30%-50%. As a whole, the probability of intra-seasonal drought in the WRB is high in the coming 30 years, but the risk of inter-seasonal drought is greater for hydrologic drought than for meteorological drought. Among them, except for the inter-seasonal RCP 4.5 scenario, the probability of hydrological drought in the upstream is greater than that of hydrological drought in the downstream, indicating that the upstream basin is more susceptible to hydrological drought. Interestingly,

the probability of intra-seasonal meteorological droughts is greater than that of intra-seasonal hydrological droughts, while that of inter-seasonal droughts is smaller than inter-seasonal hydrological droughts (except for the SJB85 scenario). This indicates that meteorological droughts tend to be intra-seasonal, while hydrological droughts tend to be inter-seasonal in the WRB in the next three decades. In other words, meteorological droughts are mostly short-term droughts, while hydrological droughts are likely to be both short-term and long-term droughts.

Table 11

Probabilistic prediction of intra-seasonal and inter-seasonal hydrological drought risk

Scenario	Copula	RMSE	AIC	BIC	θ
SJB45	Clayton-copula	0.09	-273.97	-272.47	
	Frank-copula	**0.06**	**-303.19**	**-301.69**	12.83
	Gumbel-copula	0.06	-297.97	-296.48	
	Normal-copula	0.06	-296.74	-295.24	
	t-copula	0.06	-294.66	-291.67	
SJJ45	Clayton-copula	0.19	-304.17	-302.4	
	Frank-copula	0.15	-322.4	-320.63	
	Gumbel-copula	**0.12**	**-341.49**	**-339.73**	3.36
	Normal-copula	0.12	-339.54	-337.78	
	t-copula	0.12	-340.57	-337.05	
SJB85	Clayton-copula	0.09	-191.74	-190.56	
	Frank-copula	0.07	-199.45	-198.27	
	Gumbel-copula	0.06	-205.56	-204.38	
	Normal-copula	**0.06**	**-205.66**	**-204.48**	0.92
	t-copula	0.06	-203.6	-201.24	
SJJ85	Clayton-copula	0.06	-242.75	-241.45	
	Frank-copula	0.06	-243.31	-242.01	
	Gumbel-copula	0.06	-238.51	-237.21	
	Normal-copula	**0.06**	**-243.39**	**-242.09**	0.9
	t-copula	0.06	-241.35	-238.76	

In general, precipitation, as a basic meteorological variable of the water circulation and hydrological processes, may lead to water shortages in rivers, lakes and reservoirs, and consequently to hydrological droughts. In addition to climatic factors, the impact of human activities, which change the underlying surface, on hydrological processes cannot be overlooked. Land use changes directly reflect the impact of human activities

on hydrological processes, and indirectly affect the occurrence of droughts. The analysis hydrological droughts risk shows that hydrological droughts occur more frequently in the upstream than in the downstream. Besides, the influence of underlying surface on hydrological droughts cannot be ignored, despite the extremely heavy influence of meteorological droughts on hydrological droughts. The slope may affect the propagation of drought (Xu et al., 2019; Yang et al., 2017). The upstream area is at high altitudes and mostly located at the slope of mountainous and hilly areas. Under the same circumstances, the greater the slope, the faster the flow rate, and the uneven distribution within the year in this area easily causes seasonal droughts. Additionally, the land use map of Figure 5 and Figure 6 shows that the underlying surface of the upstream area is mainly covered with woodlands and orchard. For one thing, the woodlands in the upstream basin include tropical rainforests, rubber plantations and other commercial forests. These vegetations are broad-leaved forests, which also makes the study area unique in respect of geographical and ecological vulnerability. The evapotranspiration of broad-leaved forests is higher owing to the homogeneous structure of rubber plantations as well as the large space and strong winds between trees. The literature also indicates that the evapotranspiration of forests is higher than that of grassland and cropland (Sterling et al., 2012; Xu et al., 2019). In the meantime, forest land can alter local microtopography and change the infiltration rate of water flowing into the soil and slow down or maintain streamflow, thereby increasing droughts (Chang et al., 2015). For another, fruits and cash crops grown in orchard, which are the main economic income of the region, and these tropical cash crops require sufficient water for irrigation. Further, agricultural activities need lots of water from rivers, and thus lead to drought. Following the principle of water balance, drought also occurs in case of constant precipitation and greater evaporation (Barker et al., 2016). Therefore, the probability of hydrological drought is greater in the upstream than in the downstream.

5. Discussion

5.1 Intra-seasonal and inter-seasonal droughts

The analysis of meteorological and hydrological droughts risk suggests that the probability of intra-seasonal meteorological droughts is greater than that of intra-seasonal hydrological droughts, but the probability of inter-seasonal hydrological droughts is greater than that of inter-seasonal meteorological droughts. What are the reasons behind such results? The probability of intra-seasonal meteorological droughts is greater than that of inter-seasonal ones, so the meteorological droughts in the WRB are short-term droughts. The copula joint distribution map of hydrological drought indicates that the droughts in this basin are dominated by drought severity, and that multiple discontinuous short-term meteorological drought events can be connected into one long-duration hydrological drought event. On top of that, the drought characteristics of the WRB were further analyzed by violin plot, which is a combination of box plot and kernel density plot. The box plot shows the location of quantiles, while the violin plot shows the density at any location. Therefore, we can know which locations have a higher density via the violin plot. As shown in Figure 9, the violin plot illustrates that meteorological droughts are mostly short-term droughts, whereas hydrological droughts are largely medium- and long-term droughts.

In general, hydrological droughts develop slowly and over a long period of time, and for some reasons, such as temporary precipitation, the severity of meteorological droughts is higher than the truncation level and they terminate early (Wu et al., 2017). Nonetheless, hydrological drought does not stop because its severity is still

below the truncation level. As a result, the duration of hydrological drought is longer than that of meteorological drought, which explains why meteorological drought is intra-seasonal, while hydrological drought is inter-seasonal in the WRB. This conclusion is consistent with the findings of literature review that meteorological droughts have a higher frequency and a shorter duration than those of hydrological droughts (Wu et al., 2017; Xu et al., 2019; Zhou et al., 2021). Consequently, according to the characteristics of meteorological and hydrological droughts in the WRB, corresponding measures (such as reservoir regulation, etc.) are developed to mitigate the effects of meteorological and hydrological droughts on the local ecological environment.

Figure 9 is here

5.2 Relationship between meteorological and hydrological droughts

XWT was employed for a more detailed analysis of the relationship between hydrological and meteorological droughts. Figure 10 shows the XWT between monthly SSI and SPI. In order to reduce the boundary effect of wavelet transform and high-frequency interference information, the figure used the thin solid line as the boundary of the cone of influence (COI), which is the effective spectral region, while the black thick line in the region is the significance level of 95%. Besides, the arrow represents the phase difference. To be specific, the rightwards arrow indicates that the two time series are in phase, whereas the leftwards arrow indicates that the two time series are out of phase; the upward arrow indicates that the hydrological drought precedes the meteorological one, whereas the downward arrow indicates that the hydrological drought lags behind the meteorological one. In the meantime, the bigger the wavelet transform coefficient, the higher the correlation, and the colored bar on the right denotes wavelet energy. As shown in Figure 10a, the phase angle relationship illustrates that the arrows mostly point to the right, suggesting that SSI and SPI are significantly and positively correlated on the timescale. Figure 10a-d shows the cross wavelet energy spectrum of monthly SSI and SPI series for each scenario, and that SSI and SPI are closely related in each scenario. As can be observed in Figure 10a, the significant resonance periods of SPI and SSI are 8-16 (2022-2028), 13-16 (2032-2037), 14-18 (2038-2042), and 6-18 (2045-2048), and most of the phase angles are on the bottom right in these time periods, suggesting that SSI lags behind the change of SPI during these time periods. In a nutshell, SPI strongly influences SSI with a significant positive correlation. In the same vein, the resonant frequency phase characteristics of meteorological and hydrological droughts for the other three scenarios can be obtained. On top of that, Figures 10a and 10b, and Figures 10c and 10d are highly similar. Figures 10a and 10b are RCP 4.5, while Figures 10c and 10d are RCP 8.5, so they share strong similarity. From the confidence region in the figures, it can be noted that meteorological drought has a strong phase relationship with hydrological drought, suggesting that the former exerts an extremely strong influence on the latter. Overall, the cyclical characteristics of meteorological and hydrological droughts play a leading role in those of hydrological drought.

Hydrological drought is the continuation and development of meteorological drought, so its evolutionary characteristics are closely associated with meteorological drought. Hence, PT from meteorological to hydrological drought can enhance the understanding of the relationship between meteorological and hydrological droughts and offer reference for the early warning of hydrological drought in the Wanquan River. Additionally, because of the multi-timescale characteristics of drought, a single timescale cannot accurately describe the propagation properties from meteorological drought to hydrological drought. In this paper, therefore, the maximum correlation coefficient between hydrological droughts at different timescales and

meteorological droughts at multiple timescales was examined by PCC to obtain the PT from meteorological drought to hydrological drought (Wu et al., 2018; Wu et al., 2021; Zhou et al., 2021). Figures 11(a)-(d) demonstrate the PCCs between hydrological droughts at a single timescale (1-month, 3-month, or 12-month) and meteorological droughts at different timescales (1-month to 24-month) under different scenarios. For JB4.5 and JJ4.5, the SSI at the 1-month timescale is best correlated with the SPI at the 3-month timescale; the SSI at the 3-month timescale is best correlated with the SPI at the 5-month timescale; and the SSI at the 12-month timescale is best correlated with the SPI at the 12-month timescale. The lag time of hydrological drought in this scenario was obtained from correlation analysis as follows: about 2-3 months for the 1-month timescale, 2-3 months for the 3-month timescale, and 1 month for the 12-month timescale. Similarly, for JB8.5 and JJ8.5, the SSI for the 1-month timescale is best correlated with the SPI for the 2-month timescale; the SSI for the 3-month time scale is best correlated with the SPI for the 4-month timescale; and the SSI for the 12-month time scale is best correlated with the SPI for the 12-month timescale. Therefore, the lag time is as follows: about 1-2 months for the 1-month timescale, 1-2 months for the 3-month timescale, and 1 month for the 12-month timescale. The correlations of time lags between SSI and SPI for upstream and downstream parts are relatively consistent across the four scenarios, which reflects the consistency of response thresholds of hydrological droughts to meteorological droughts in the same climate regions. It is noteworthy that the response thresholds of hydrological droughts to meteorological droughts are different in the two different RCP scenarios. In addition, it can also be observed from Figure 11 that the correlation coefficients between hydrological and meteorological droughts are larger in the RCP45 scenario than in the RCP85 scenario, and that the response thresholds of hydrological droughts to meteorological droughts are higher in the RCP45 scenario than in the RCP85 scenario, which is ascribed to the differences between the two climate models. Compared to the RCP45 scenario, the RCP85 scenario is the baseline scenario without interventions from climate change policy, a scenario where human activities contribute to a maximum GHG concentration. In the meantime, the frequency and intensity of extreme weather events increase, and changes in temperature and precipitation alter the process of hydrological cycle and thus that of drought propagation (Xu et al., 2015; Yang et al., 2018). Therefore, the response threshold of hydrological droughts to meteorological droughts is higher in the RCP45 scenario than in the RCP85 scenario. As a whole, the results of XWT and correlation analysis indicate that there is a stable relationship between meteorological and hydrological drought in the WRB, and determining the reasonableness of the PT from hydrological to meteorological drought is of great value for detection and early warning of future regional drought.

Figure 10 is here

Figure 11 is here

6. Conclusions

Prediction of meteorological and hydrological drought risk is of vital importance as it is a basis for early warning of drought and helps to develop effective measures to minimize the damage from future droughts. In this study, the daily precipitation and daily maximum and minimum temperatures of RCP4.5 and RCP8.5 scenarios for 2021-2050 were extracted based on the NEX-GDDP. Besides, a CA-Markov model was applied to simulate and predict future land use changes in the WRB. Furthermore, based on the future climate scenarios and land use, the SWAT model was employed to simulate future streamflow, and the copula function was used

to predict meteorological and hydrological droughts risk of intra-season and inter-season in the basin. Finally, the relationship between meteorological and hydrological drought was analyzed. The results are as follow:

(1) The CA-Markov model can better simulate LULC maps for 2000 and 2010, so the future LULC maps for 2030, 2040 and 2050 could be predicted based on the validated CA-Markov model, comparing with land use in 2015, land use in 2030, 2040 and 2050 is basically the same in overall spatial distribution, but there are obvious changes in each land use type within them. (2) The simulation results of the SWAT model were more desirable through calibration and validation of two hydrological stations, so future streamflow can be predicted based on the parameters of the validated SWAT model. (3) Subsequently, SPI and SSI were calculated based on the input and output data of SWAT, and the run theory was adopted to extract the drought characteristics and fit the marginal distribution for drought duration and severity. The correlation coefficients of both drought duration and severity are greater than 0.68, suggesting that they are well correlated and can be used to construct binary copula functions. Meanwhile, the GOF for copulas performed well for each scenario in this basin. (4) The WRB is prone to intra-seasonal meteorological droughts in the next 30 years (2021-2050) with a probability of 40%-70%, whereas the probability of inter-seasonal hydrological drought is smaller. Furthermore, the risk of inter-seasonal hydrological droughts in this basin is higher (30%-50%) than that of meteorological drought. Besides, the risk of hydrological drought is higher in the upstream than in the downstream. The upstream area is mostly located in mountainous and hilly areas, and is endowed with abundant tropical rainforests and rubber plantations, so it has distinctive geographical and ecological vulnerability, and hydrological drought lags behind meteorological drought in this area. For these reasons, relevant departments should adopt appropriate measures to prevent drought hazards.

Declarations

Acknowledgements

This study was supported by the National Natural Science Foundation of China (Grant Nos. 52179029 and 51879289), the Innovation Fund of Guangzhou City water science and technology (GZSWKJ-2020-2) and the Guangdong Basic and Applied Basic Research Foundation (2019B1515120052).

Author Contributions

Dan Li: Methodology, Software, Validation, Investigation, Visualization, Writing - original draft. **Bingjun Liu**: Conceptualization; funding acquisition; project administration; supervision. **Changqing Ye**: Resources, Investigation, validation; writing-original draft.

Conflicts of Interest:

The authors declare no conflict of interest.

References

1. Ayantobo, O.O., Wei, J., Wang, G., 2021. Modeling Joint Relationship and Design Scenarios Between Precipitation, Surface Temperature, and Atmospheric Precipitable Water Over Mainland China. Earth and Space Science 8. https://doi.org/10.1029/2020ea001513

2. Barker, L.J., Hannaford, J., Chiverton, A., Svensson, C., 2016. From meteorological to hydrological drought using standardised indicators. Hydrology and Earth System Sciences 20, 2483–2505. https://doi.org/10.5194/hess-20-2483-2016
3. Chang, J., Li, Y., Wang, Y., Yuan, M., 2016. Copula-based drought risk assessment combined with an integrated index in the Wei River Basin, China. Journal of Hydrology 540, 824–834. https://doi.org/10.1016/j.jhydrol.2016.06.064
4. Chang, J., Wang, Y., Istanbulluoglu, E., Bai, T., Huang, Q., Yang, D., Huang, S., 2015. Impact of climate change and human activities on runoff in the Weihe River Basin, China. Quaternary International 380–381, 169–179. https://doi.org/10.1016/j.quaint.2014.03.048
5. Ghosh, P., Mukhopadhyay, A., Chanda, A., Mondal, P., Akhand, A., Mukherjee, S., Nayak, S.K., Ghosh, S., Mitra, D., Ghosh, T., Hazra, S., 2017. Application of Cellular automata and Markov-chain model in geospatial environmental modeling- A review. Remote Sensing Applications: Society and Environment 5, 64–77. https://doi.org/10.1016/j.rsase.2017.01.005
6. Gu, L., Chen, J., Yin, J., Xu, C.-Y., Chen, H., 2020. Drought hazard transferability from meteorological to hydrological propagation. Journal of Hydrology 585. https://doi.org/10.1016/j.jhydrol.2020.124761
7. Halmy, M.W.A., Gessler, P.E., Hicke, J.A., Salem, B.B., 2015. Land use/land cover change detection and prediction in the north-western coastal desert of Egypt using Markov-CA. Applied Geography 63, 101–112. https://doi.org/10.1016/j.apgeog.2015.06.015
8. Huang, L., Zhou, P., Cheng, L., Liu, Z., 2021. Dynamic drought recovery patterns over the Yangtze River Basin. CATENA 201, 105194. https://doi.org/10.1016/j.catena.2021.105194
9. Huang, S., Li, P., Huang, Q., Leng, G., Hou, B., Ma, L., 2017. The propagation from meteorological to hydrological drought and its potential influence factors. Journal of Hydrology 547, 184–195. https://doi.org/10.1016/j.jhydrol.2017.01.041
10. Li, Y., Luo, L., Chang, J., Wang, Y., Guo, A., Fan, J., Liu, Q., 2020. Hydrological drought evolution with a nonlinear joint index in regions with significant changes in underlying surface. Journal of Hydrology 585, 124794. https://doi.org/10.1016/j.jhydrol.2020.124794
11. Lin, K., Lin, Y., Xu, Y., Chen, X., Chen, L., Singh, V.P., 2017. Inter- and intra- annual environmental flow alteration and its implication in the Pearl River Delta, South China. Journal of Hydro-environment Research 15, 27–40. https://doi.org/10.1016/j.jher.2017.01.002
12. Lorenzo-Lacruz, J., Vicente-Serrano, S.M., González-Hidalgo, J.C., López-Moreno, J.I., Cortesi, N., 2013. Hydrological drought response to meteorological drought in the Iberian Peninsula. Climate Research 58, 117–131. https://doi.org/10.3354/cr01177
13. Mishra, A.K., Singh, V.P., 2010. A review of drought concepts. Journal of Hydrology 391, 202–216. https://doi.org/10.1016/j.jhydrol.2010.07.012
14. Parry, S., Prudhomme, C., Wilby, R.L., Wood, P.J., 2016a. Drought termination: Concept and characterisation. Progress in Physical Geography: Earth and Environment 40, 743–767. https://doi.org/10.1177/0309133316652801
15. Parry, S., Wilby, R.L., Prudhomme, C., Wood, P.J., 2016b. A systematic assessment of drought termination in the United Kingdom. Hydrol. Earth Syst. Sci. 20, 4265–4281. https://doi.org/10.5194/hess-20-4265-2016

16. Rajsekhar, D., Singh, Vijay.P., Mishra, Ashok.K., 2015. Multivariate drought index: An information theory based approach for integrated drought assessment. Journal of Hydrology 526, 164–182. https://doi.org/10.1016/j.jhydrol.2014.11.031
17. Sadegh, M., Ragno, E., AghaKouchak, A., 2017. Multivariate Copula Analysis Toolbox (MvCAT): Describing dependence and underlying uncertainty using a Bayesian framework. Water Resources Research 53, 5166–5183. https://doi.org/10.1002/2016wr020242
18. Shiau, J.T., 2006. Fitting Drought Duration and Severity with Two-Dimensional Copulas. Water Resources Management 20, 795–815. https://doi.org/10.1007/s11269-005-9008-9
19. Sterling, S.M., Ducharne, A., Polcher, J., 2012. The impact of global land-cover change on the terrestrial water cycle. Nature Climate Change 3, 385–390. https://doi.org/10.1038/nclimate1690
20. Sun, F., Mejia, A., Zeng, P., Che, Y., 2019. Projecting meteorological, hydrological and agricultural droughts for the Yangtze River basin. Science of The Total Environment 696. https://doi.org/10.1016/j.scitotenv.2019.134076
21. Taylor, K.E., Stouffer, R.J., Meehl, G.A., 2012. An Overview of CMIP5 and the Experiment Design. Bulletin of the American Meteorological Society 93, 485–498. https://doi.org/10.1175/bams-d-11-00094.1
22. Van Loon, A.F., 2013. On the propagation of drought. How climate and catchment characteristics influence hydrological drought development and recovery. Wageningen University, Wageningen, The Netherlands (April), 198.
23. Van Loon, A.F., Stahl, K., Di Baldassarre, G., Clark, J., Rangecroft, S., Wanders, N., Gleeson, T., Van Dijk, A.I.J.M., Tallaksen, L.M., Hannaford, J., Uijlenhoet, R., Teuling, A.J., Hannah, D.M., Sheffield, J., Svoboda, M., Verbeiren, B., Wagener, T., Van Lanen, H.A.J., 2016. Drought in a human-modified world: reframing drought definitions, understanding, and analysis approaches. Hydrology and Earth System Sciences 20, 3631–3650. https://doi.org/10.5194/hess-20-3631-2016
24. Wang, F., Wang, Z., Yang, H., Di, D., Zhao, Y., Liang, Q., Hussain, Z., 2020. Comprehensive evaluation of hydrological drought and its relationships with meteorological drought in the Yellow River basin, China. Journal of Hydrology 584. https://doi.org/10.1016/j.jhydrol.2020.124751
25. Wickramasuriya, R.C., Bregt, A.K., van Delden, H., Hagen-Zanker, A., 2009. The dynamics of shifting cultivation captured in an extended Constrained Cellular Automata land use model. Ecological Modelling 220, 2302–2309. https://doi.org/10.1016/j.ecolmodel.2009.05.021
26. Williams, A.P., Cook, E.R., Smerdon, J.E., Cook, B.I., Abatzoglou, J.T., Bolles, K., Baek, S.H., Badger, A.M., Livneh, B., 2020. Large contribution from anthropogenic warming to an emerging North American megadrought. Science 368, 314–318. https://doi.org/10.1126/science.aaz9600
27. Wu, J., Chen, X., Yao, H., Gao, L., Chen, Y., Liu, M., 2017. Non-linear relationship of hydrological drought responding to meteorological drought and impact of a large reservoir. Journal of Hydrology 551, 495–507. https://doi.org/10.1016/j.jhydrol.2017.06.029
28. Wu, J., Chen, X., Yao, H., Liu, Z., Zhang, D., 2018a. Hydrological Drought Instantaneous Propagation Speed Based on the Variable Motion Relationship of Speed-Time Process. Water Resour. Res. 54, 9549–9565. https://doi.org/10.1029/2018WR023120
29. Wu, J., Chen, X., Yao, H., Zhang, D., 2021. Multi-timescale assessment of propagation thresholds from meteorological to hydrological drought. Sci Total Environ 765, 144232.

https://doi.org/10.1016/j.scitotenv.2020.144232

30. Wu, J., Chen, X., Yu, Z., Yao, H., Li, W., Zhang, D., 2019. Assessing the impact of human regulations on hydrological drought development and recovery based on a 'simulated-observed' comparison of the SWAT model. Journal of Hydrology 577, 123990. https://doi.org/10.1016/j.jhydrol.2019.123990
31. Wu, J., Liu, Z., Yao, H., Chen, Xiaohong, Chen, Xingwei, Zheng, Y., He, Y., 2018b. Impacts of reservoir operations on multi-scale correlations between hydrological drought and meteorological drought. Journal of Hydrology 563, 726–736. https://doi.org/10.1016/j.jhydrol.2018.06.053
32. Wu, Jingwen., Miao, C., Zheng, H., Duan, Q., Lei, X., Li, H., 2018. Meteorological and Hydrological Drought on the Loess Plateau, China: Evolutionary Characteristics, Impact, and Propagation. Journal of Geophysical Research: Atmospheres 123, 11,569-11,584. https://doi.org/10.1029/2018jd029145
33. Xu, K., Yang, D., Xu, X., Lei, H., 2015. Copula based drought frequency analysis considering the spatio-temporal variability in Southwest China. Journal of Hydrology 527, 630–640. https://doi.org/10.1016/j.jhydrol.2015.05.030
34. Xu, Y., Zhang, X., Wang, X., Hao, Z., Singh, V.P., Hao, F., 2019. Propagation from meteorological drought to hydrological drought under the impact of human activities: A case study in northern China. Journal of Hydrology 579. https://doi.org/10.1016/j.jhydrol.2019.124147
35. Yang, X., Wood, E.F., Sheffield, J., Ren, L., Zhang, M., Wang, Y., 2018. Bias Correction of Historical and Future Simulations of Precipitation and Temperature for China from CMIP5 Models. Journal of Hydrometeorology 19, 609–623. https://doi.org/10.1175/jhm-d-17-0180.1
36. Yang, Y., McVicar, T.R., Donohue, R.J., Zhang, Y., Roderick, M.L., Chiew, F.H.S., Zhang, L., Zhang, J., 2017. Lags in hydrologic recovery following an extreme drought: Assessing the roles of climate and catchment characteristics. Water Resources Research 53, 4821–4837. https://doi.org/10.1002/2017wr020683
37. Zhang, B., Wang, S., Wang, Y., 2019. Copula-Based Convection-Permitting Projections of Future Changes in Multivariate Drought Characteristics. Journal of Geophysical Research: Atmospheres 124, 7460–7483. https://doi.org/10.1029/2019jd030686
38. Zhang, D., Chen, X., Yao, H., Lin, B., 2015. Improved calibration scheme of SWAT by separating wet and dry seasons. Ecological Modelling 301, 54–61. https://doi.org/10.1016/j.ecolmodel.2015.01.018
39. Zhang, D., Zhang, Q., Werner, A.D., Liu, X., 2016. GRACE-Based Hydrological Drought Evaluation of the Yangtze River Basin, China. Journal of Hydrometeorology 17, 811–828. https://doi.org/10.1175/JHM-D-15-0084.1
40. Zhang, X., Zhou, J., Song, W., 2020. Simulating Urban Sprawl in China Based on the Artificial Neural Network-Cellular Automata-Markov Model. Sustainability 12. https://doi.org/10.3390/su12114341
41. Zhao, Y., Zou, X., Liu, Q., Chen, Y., 2019. Impacts of Climate Variability and Human Activities on Streamflow in the Wanquan River Basin along the East Coast of Hainan Island, Southern China. Journal of Coastal Research 35. https://doi.org/10.2112/jcoastres-d-18-00005.1
42. Zhou, Z., Shi, H., Fu, Q., Ding, Y., Li, T., Wang, Y., Liu, S., 2021. Characteristics of Propagation From Meteorological Drought to Hydrological Drought in the Pearl River Basin. Journal of Geophysical Research: Atmospheres 126.

Figures

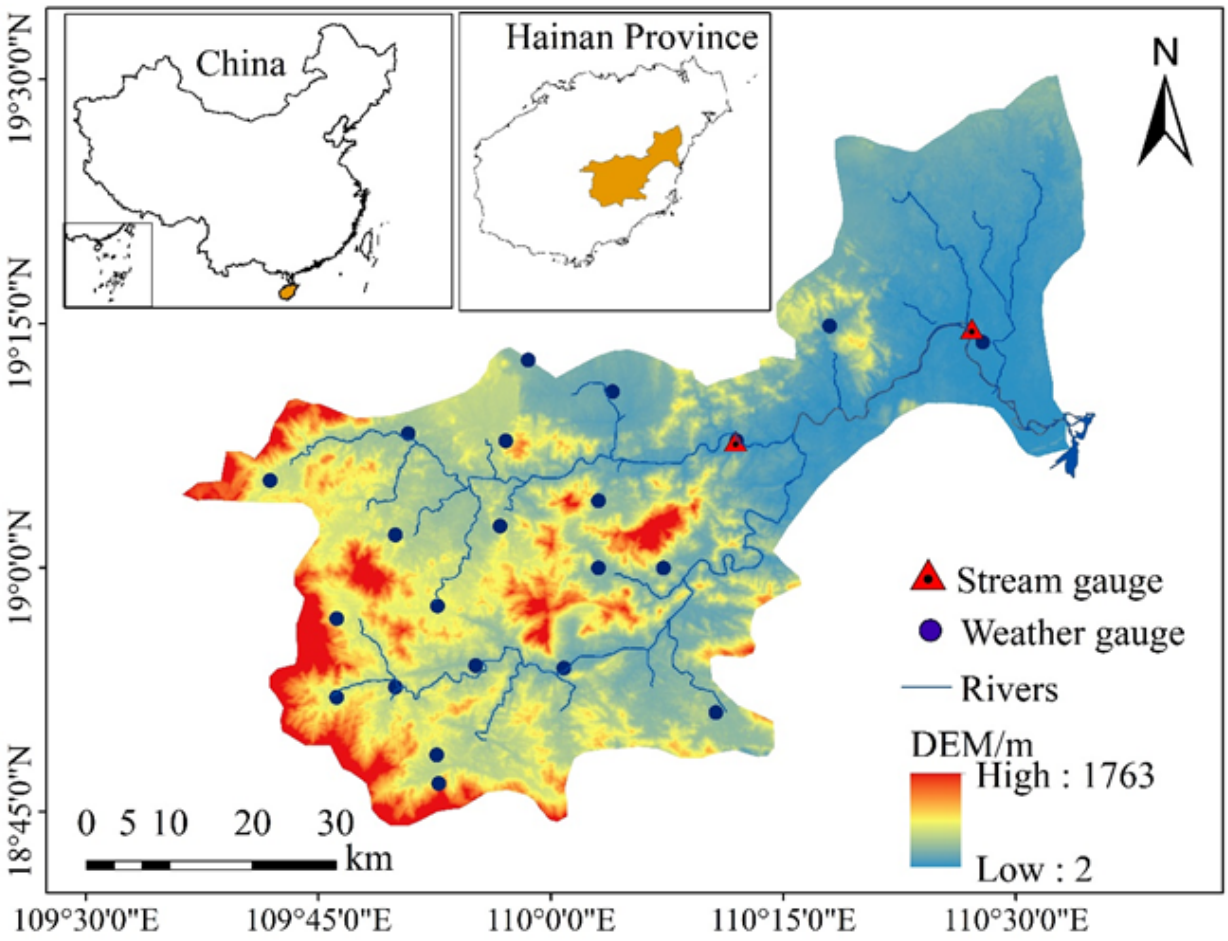

Figure 1

Location of the WRB and spatial distribution of hydrological and meteorological station

Figure 2

Flow chart of this study

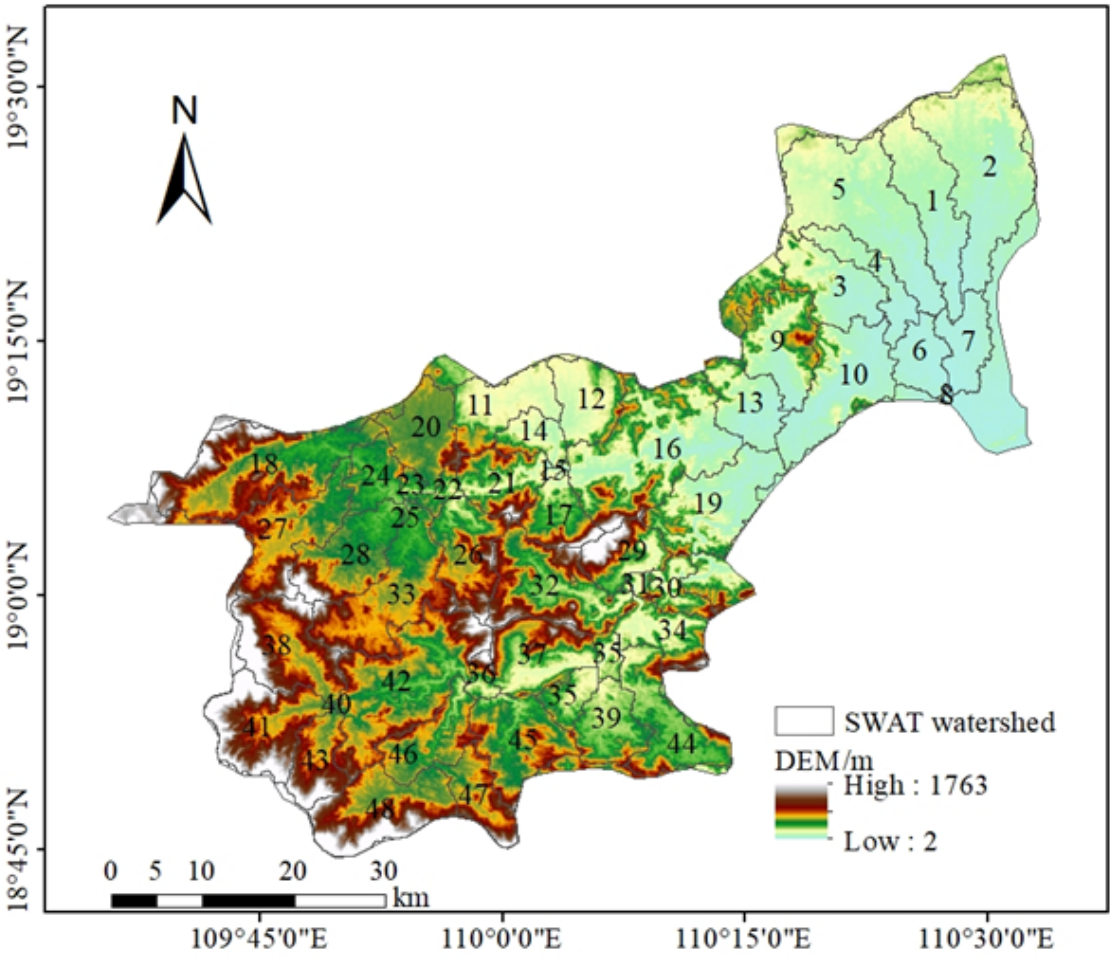

Figure 3

Sub-watersheds delineated by the SWAT model

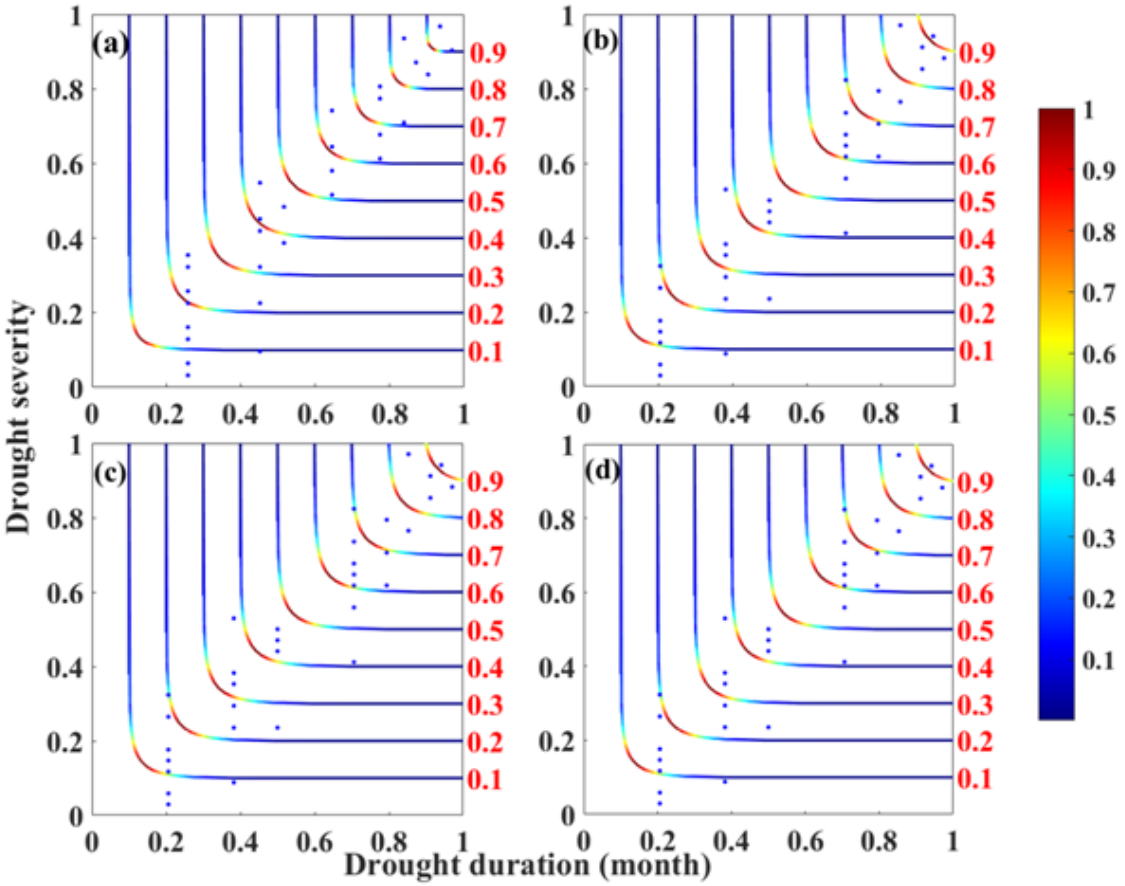

Figure 4

Probabilistic contours of correlation between meteorological drought duration and severity

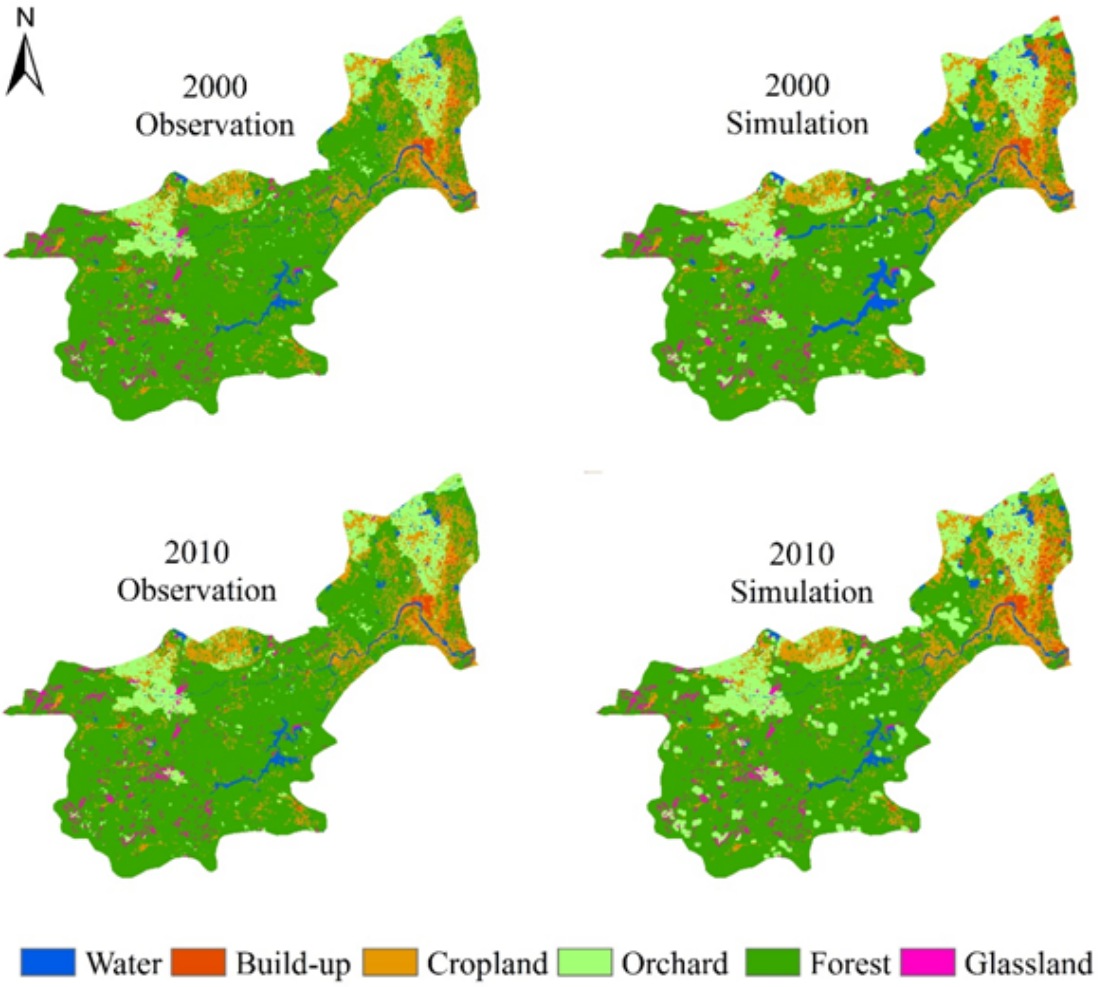

Figure 5

Simulated land use maps of 2000 and 2010

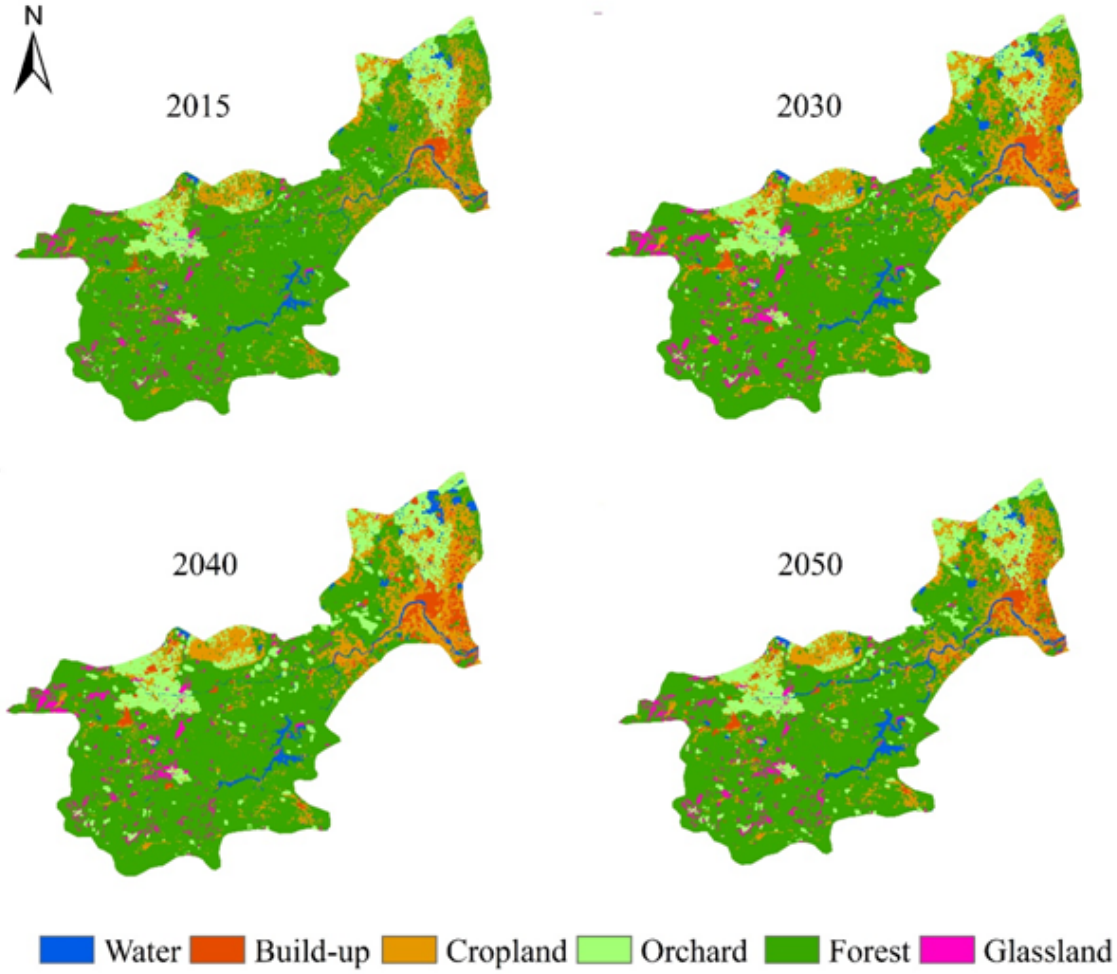

Figure 6

Projected spatial distribution map of LULC in 2030, 2040 and 2050 in the WRB

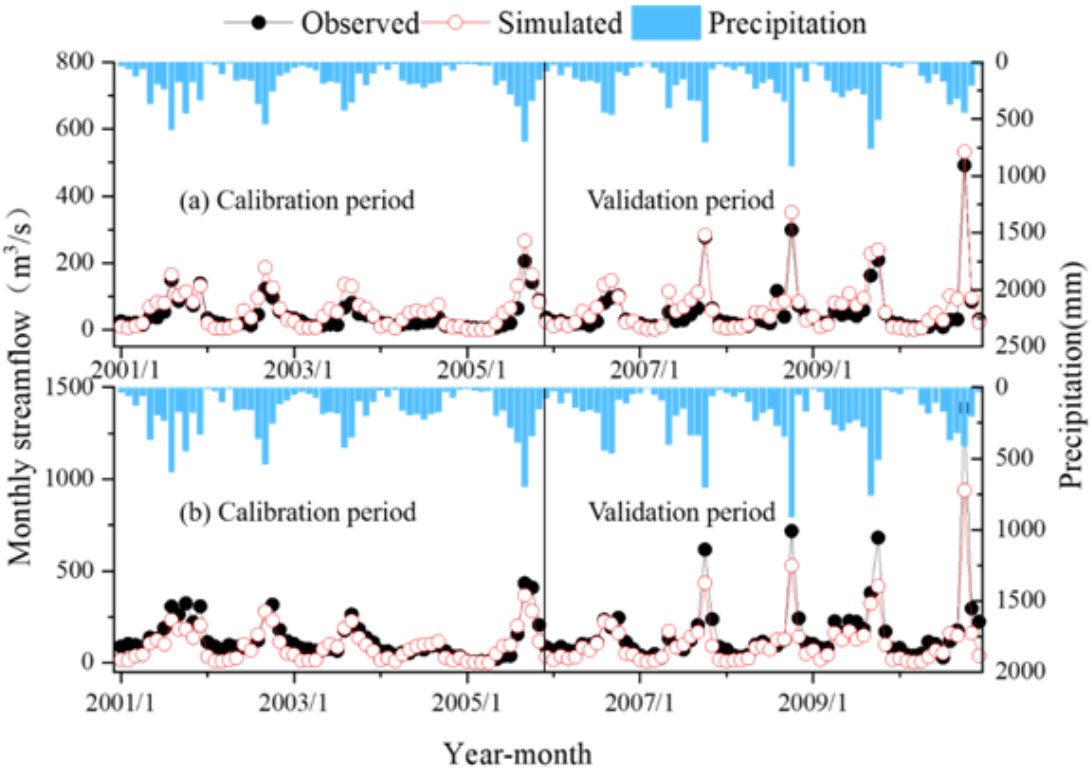

Figure 7

Comparison of precipitation, streamflow and simulated streamflow for two stations during the calibration and validation periods

Figure 8

Probabilistic contours of correlation between hydrological drought duration and severity

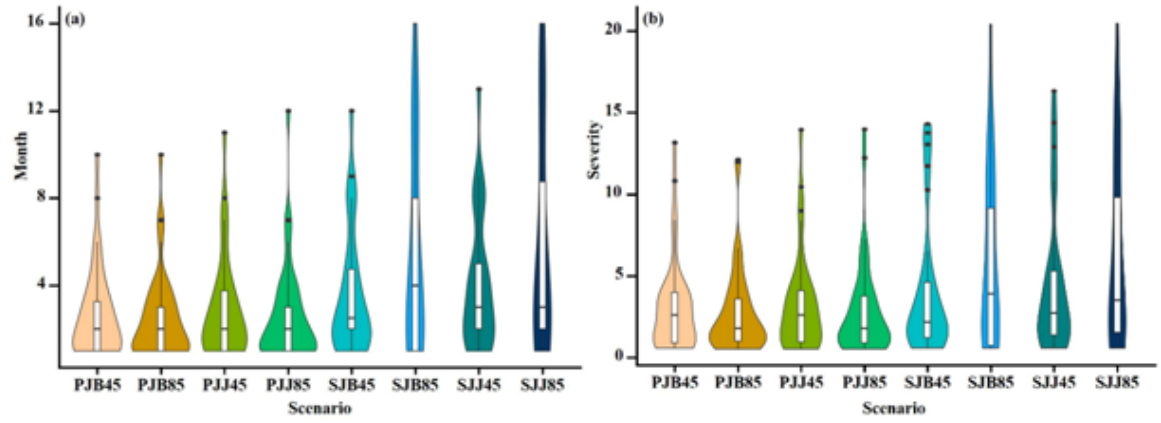

Figure 9

Drought characteristics (drought duration and severity)

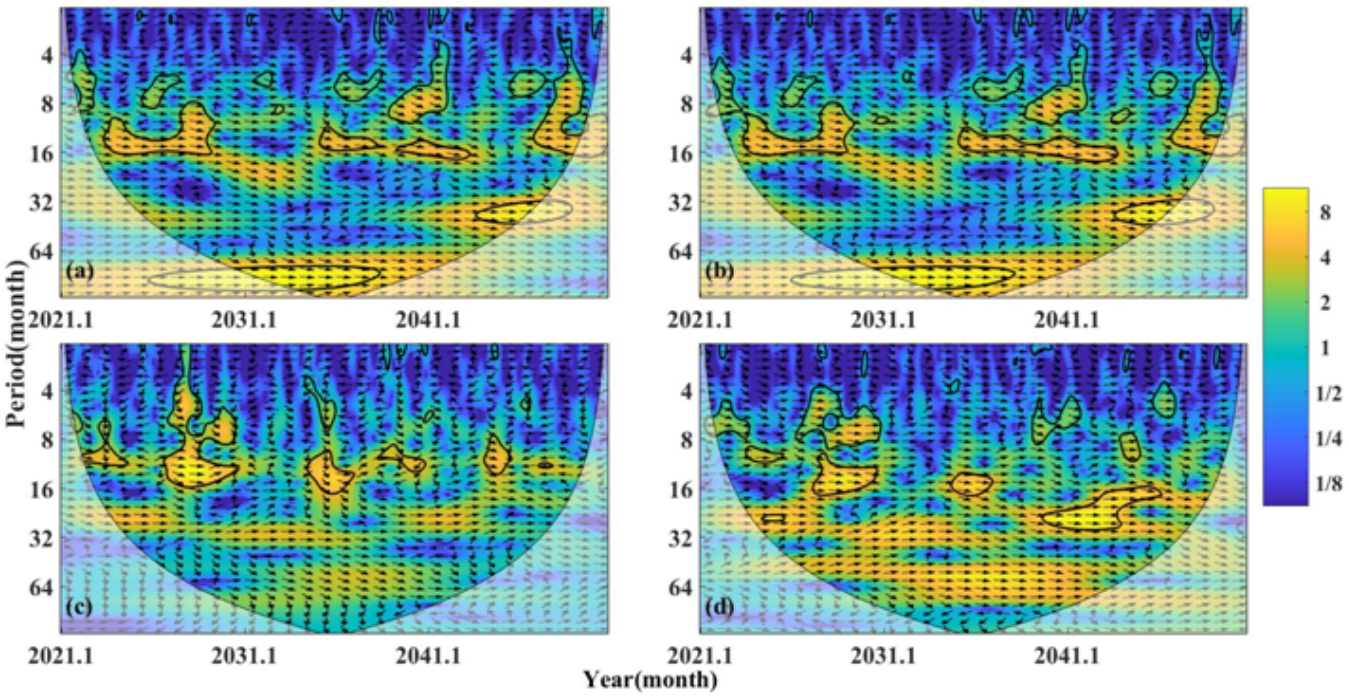

Figure 10

XWT between the monthly SSI and SPI series at different scales in different scenarios (a: JB45, b: JJ45, c: JB85, d: JJ85)

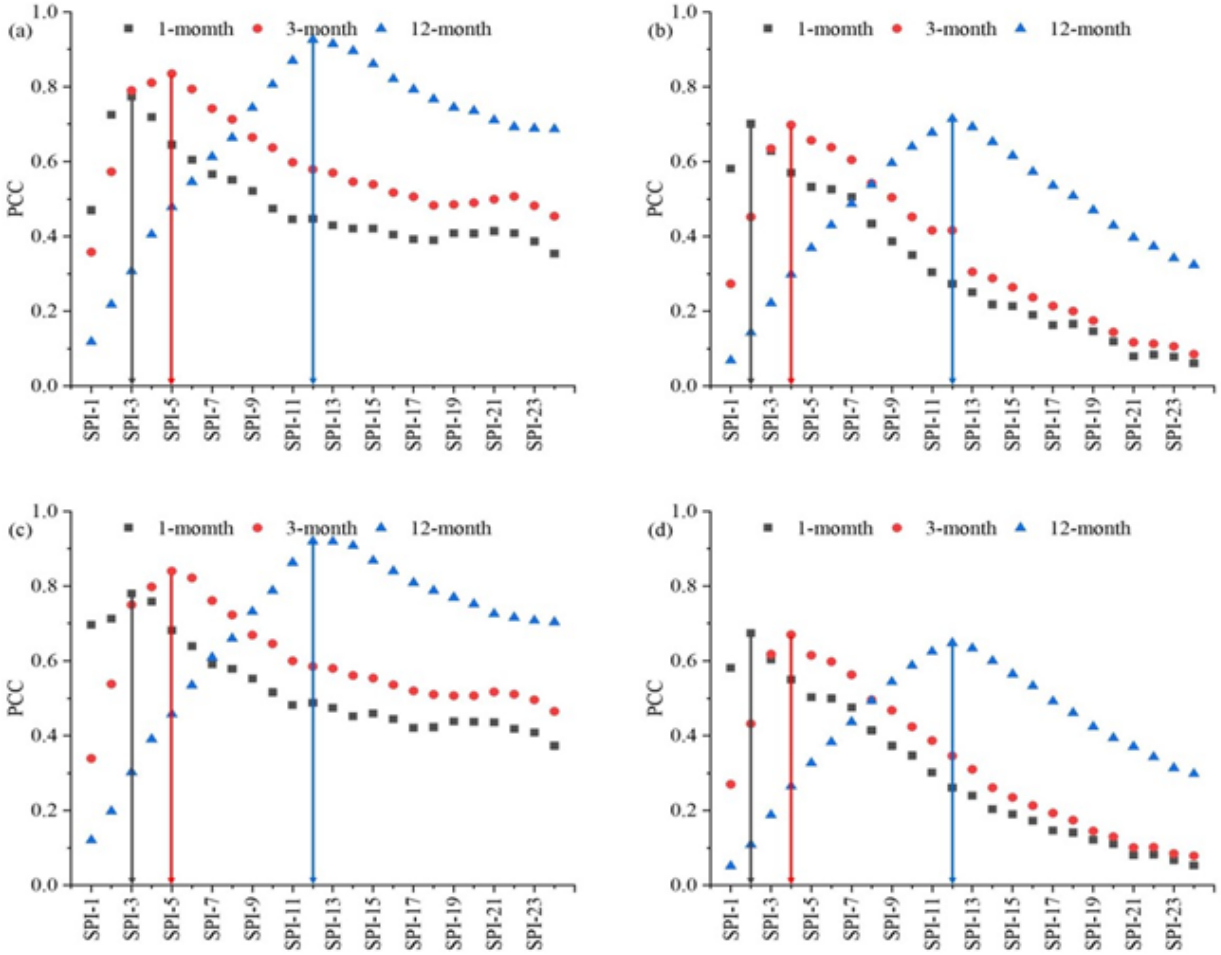

Figure 11

Correlation between SSI at a single timescale and SPI at different timescales in different scenarios (a: JB45, b: JJ45, c: JB85, d: JJ85)